Prepared for submission to JCAP

Revisiting cosmic ray antinuclei fluxes with a new coalescence model

M. Kachelrieß,[a] **S. Ostapchenko,**[b,c] **J. Tjemsland**[a]

[a]Institutt for fysikk, NTNU, Trondheim, Norway
[b]Frankfurt Institute for Advanced Studies, Frankfurt, Germany
[c]D. V. Skoveltsyn Institute of Nuclear Physics, Moscow State University, Moscow, Russia

Abstract. Antideuteron and antihelium nuclei have been proposed as promising detection channels for dark matter because of the low astrophysical backgrounds expected. To estimate both potential exotic contributions and their backgrounds, one usually employs the coalescence model in momentum space. Here we use instead a newly developed coalescence model based on the Wigner function representations of the produced nuclei states. This approach includes both the process-dependent size of the formation region of antinuclei, and the momentum correlations of coalescing antinucleons in a semi-classical picture. The model contains a single universal parameter σ that we tune to experimental data on antideuteron production in electron-positron, proton-proton and proton-nucleus collisions. The obtained value $\sigma \simeq 1\,\mathrm{fm}$ agrees well with its physical interpretation as the size of the formation region of antinuclei in collisions of point-like particles. This model allows us therefore to calculate in a consistent frame-work the antideuteron and antihelium fluxes both from secondary production and from dark matter annihilations. We find that the antihelium-3 flux falls short by more than an order of magnitude of the detection sensitivity of the AMS-02 experiment, assuming standard cosmic ray propagation parameters, while the antideuteron flux can be comparable to the sensitivities of the AMS-02 and GAPS experiments.

Keywords: antideuteron, antihelium, dark matter, secondary production, coalescence model

Contents

1 Introduction

The low astrophysical backgrounds promote antideuteron [1] and antihelium-3 [2] nuclei to promising detection channels for dark matter (DM) annihilations and decays in the Galaxy, for a recent review see Ref. [3]. The dominant background of light antinuclei is expected to originate from secondary production, that is, to be created in collisions of primary cosmic rays (CR) with the interstellar medium. The high threshold energy for the production of antideuterons ($\simeq 17 m_N$ in pp interactions, where m_N is the nucleon mass) and antihelium-3 ($\simeq 31 m_N$) implies that such secondary antinuclei have relatively high kinetic energies. This makes antideuterons and antihelium-3 with low kinetic energies an ideal dark matter probe. In contrast, the fluxes of heavier nuclei, as e.g. antihelium-4, are, both for the DM and secondary production channels, so strongly suppressed that they are undetectable by current experiments. Consequently, an identification of antihelium-4 nuclei in the Galactic CR flux would represent a true challenge to our current cosmological paradigm, requiring e.g. the presence of antimatter "islands" inside the Milky Way [4, 5].

The production of light antinuclei as CR secondaries and in DM annihilations is usually described by the coalescence model in momentum space [4, 6, 7]. It states that an antiproton-antineutron pair with an invariant momentum difference Δk less than the coalescence momentum p_0 merges and forms an antideuteron. Due to the lack of an underlying microphysical picture, p_0 must be determined by fits to experimental data. For the model to be predictive, this parameter should be independent of both the reaction type and the center-of-mass (cm) energy $\sqrt{s}$. Traditionally, the cluster formation of nuclei has been parametrised by an invariant coalescence factor B_A as

$$E_A \frac{\mathrm{d}^3 N_A}{\mathrm{d}P_A^3} = B_A \left(E_p \frac{\mathrm{d}^3 N_p}{\mathrm{d}P_p^3} \right)^Z \left(E_n \frac{\mathrm{d}^3 N_n}{\mathrm{d}P_n^3} \right)^N \Bigg|_{P_p = P_n = P_A/A} , \tag{1.1}$$

which relates the invariant differential yield of a nucleus with mass number A, proton number Z and neutron number N to the invariant yields of protons and neutrons, $E_i\,\mathrm{d}^3N_i/\mathrm{d}P_i^3$. In the limit of isotropic nucleon yields, the coalescence factor B_A is related to the coalescence momentum p_0 as

$$B_A = A\left(\frac{4\pi}{3}\frac{p_0^3}{m_N}\right)^{A-1}. \tag{1.2}$$

This "naive" coalescence model can be improved by taking into account two-particle momentum correlations provided by Monte Carlo event generators, if one imposes the coalescence condition on an event-by-event basis, as first proposed in Refs. [8, 9]. The yield of antinuclei should, however, depend on the full *phase space density* of the coalescing antinucleons. Since both the "naive" and the "improved" coalescence models impose the coalescence condition only in momentum space, the reaction-dependent size of the formation region of antinuclei is neglected in these treatments. As a result, the coalescence parameter p_0 becomes process dependent applying such models also to hadronic reactions [10–12]. Using in such an approach the same p_0 for antinuclei formation in DM annihilations and in CR interactions will thus lead to incorrect results.

An alternative coalescence model was developed by us in Ref. [13]. Starting from the Wigner function representation of the antinucleon and the antinuclei states, introduced in Ref. [14], we employed a semi-classical treatment to include both the process-dependent size of the formation region and the momentum correlations of coalescing antinucleons. We showed that this new coalescence model successfully describes the data both from e^+e^- annihilations at the Z resonance [15, 16] and from pp collisions at $\sqrt{s} = 0.9, 2.7$ and 7 TeV, measured by the ALICE collaboration at the LHC [17]. As we aim in the present work to model the formation of light antinuclei as secondaries in CR interactions, it is, however, important to test the validity of our model also in hadron-nucleus and light nucleus-nucleus collisions. We consider therefore in addition experimental data on proton-beryllium and proton-aluminium collisions at 200 GeV/c [18, 19] as well as the spectra of antinuclei for pp collisions at $\sqrt{s} = 53$ GeV measured at the CERN ISR [20, 21]. The numerical values we derive for the single free parameter σ of our model are consistent between all the reactions considered and agree well with the physical interpretation of σ as the size of the formation region of light nuclei. This allows us to calculate in a self-consistent frame-work the expected fluxes of both antideuteron and antihelium-3 from secondary production as well as from DM annihilations. In the latter case, we estimate the antinuclei flux from DM particles with masses $m_\chi = \{20, 100, 1000\}$ GeV, annihilating into $b\bar{b}$ and W^+W^- pairs. We derive also the maximal annihilation cross sections compatible with the antiproton spectrum from AMS-02. We show that pHe and HeHe collisions dominate the secondary contribution to the antideuteron yield at low energies. The antihelium-3 flux we obtain falls short of the detection sensitivities of the AMS-02 experiment by more than an order of magnitude, assuming standard CR propagation parameters. In contrast, the antideuteron flux can be just below the sensitivities of the AMS-02 and GAPS experiments. Taking into account the large uncertainties, antideuterons remain therefore a promising target in searches for antimatter.

2 Antinuclei formation model

Our formalism for treating the production of (anti)nuclei[1] has been described in Ref. [13]. We will follow the same approach here and refer the reader for details like cuts to exclude long-lived resonances to our previous work [13]. In this model, the probability that a nucleon pair with three-momentum $\boldsymbol{q}$ and $-\boldsymbol{q}$ in its cm frame coalesces is given by

$$w_{\mathrm{Wigner}} = 3\left(\zeta_1\Delta e^{-q^2d_1^2} + \zeta_2[1-\Delta]e^{-q^2d_2^2}\right), \tag{2.1}$$

where

$$\zeta_i = \frac{d_i^2}{d_i^2 + 4\tilde{\sigma}_\perp^2}\sqrt{\frac{d_i^2}{d_i^2 + 4\sigma_\parallel^2}}. \tag{2.2}$$

[1] Since our discussion applies equally well to the formation of nuclei and of antinuclei, we will omit the preposition 'anti' further on in this section.

The parameters $\Delta = 0.581$, $d_1 = 3.979\,\text{fm}$, and $d_2 = 0.890\,\text{fm}$ determine the internal wave-function of the deuteron, which was approximated in Ref. [13] as a sum of two Gaussians[2]. Since the coalescence probability is very small, corrections to Eq. (2.1), accounting for double counting of nucleons involved in different pairs, can in practice be neglected. An expression similar to Eq. (2.1) has been obtained in Ref. [13] for the probability of three nucleons to form a bound-state, like tritium or antihelium-3.

The parameters σ_i describe the spatial separation of the nucleons forming potentially a deuteron. For a "point-like" interaction, such as e^+e^- annihilations, the longitudinal spread $\sigma_\parallel$ is given in the deuteron frame by the formation length of nucleons, $\sigma_\parallel \simeq R_p \simeq 1\,\text{fm}$, with R_p as the proton size, while the perpendicular spread is of order $\sigma_\perp \simeq 1/\Lambda_{\text{QCD}}$ in the cm frame of the collision. Taking into account for the latter the boost into the deuteron frame gives

$$\tilde{\sigma}_\perp^2 = \frac{\sigma_\perp^2}{\cos^2\vartheta + \gamma^2 \sin^2\vartheta}, \tag{2.3}$$

where γ is the usual Lorentz factor, while ϑ denotes the angle between the antideuteron momentum and the momentum of the initially produced pair of particles in their cm frame. For instance, in the case of the annihilation of DM particles through the process $\chi\chi \to \bar{b}b$, the angle ϑ is defined with respect to the momentum of the produced b or $\bar{b}$. For hadronic events, ϑ is defined relative to the beam direction of the colliding hadrons in their cm system, as detailed in Ref. [13].

In addition, the spreads σ_i obtain a geometrical contribution σ_{geom} in reactions involving hadrons or nuclei because of their finite extension. Adding these two contributions in quadrature yields

$$\sigma_\perp^2 = \sigma_{\perp(e^\pm)}^2 + \sigma_{\perp(\text{geom})}^2, \tag{2.4}$$

$$\sigma_\parallel^2 = \sigma_{\parallel(e^\pm)}^2 + \sigma_{\parallel(\text{geom})}^2. \tag{2.5}$$

Here, we have denoted with $\sigma_{(e^\pm)}$ the "point-like" contribution discussed above and set for simplicity $\sigma_{(e^\pm)} \simeq \sigma_{\perp(e^\pm)} \simeq \sigma_{\parallel(e^\pm)} \simeq 5\,\text{GeV}^{-1} \simeq 1\,\text{fm}$. The geometrical contributions in hadron-hadron, hadron-nucleus, and nucleus-nucleus collisions can in turn be approximated by [13]

$$\sigma_{\perp(\text{geom})}^2 \simeq \frac{2R_1^2 R_2^2}{R_1^2 + R_2^2}, \tag{2.6}$$

$$\sigma_{\parallel(\text{geom})}^2 \simeq \max\{R_1^2, R_2^2\}, \tag{2.7}$$

where R_i are the radii of the two colliding particles. In the particular case of proton-proton collisions, $\sigma_\parallel \simeq \sigma_\perp$ so that $\sigma_{(pp)} \simeq \sqrt{2}\sigma_{(e^\pm)} \simeq 7\,\text{GeV}^{-1}$. The radius R_A of a nucleus with mass number A scales approximately as

$$R_A = a_0 A^{1/3}, \tag{2.8}$$

where $a_0 \simeq 1.1\,\text{fm}$, with an uncertainty of $\sim 20\%$ [22]. We will use this relation in Eqs. (2.6) and (2.7) as an approximation for the size of the different nuclei considered. This allows us to use a single parameter, setting

$$\sigma \equiv \sigma_{(e^\pm)} = a_0 = \sigma_{(pp)}/\sqrt{2}. \tag{2.9}$$

If our model accounts correctly for the differences in the formation of light nuclei in different reaction types, the parameter σ obtained from fits of different reactions should be universal and close to 1 fm.

Finally, we want to comment briefly on the relation of our model to other approaches. The recent work [23] connects the production of light antinuclei to the two-proton correlation function measured in heavy-ion collisions. Its basic results can be recovered in our approach imposing two assumptions: First, the size of the production region has to be much larger than the deuteron size. Second, the proton-neutron density matrix has to factorise, i.e. their momentum correlations should be negligible. Neither of the two assumptions are justified for the small systems, as pp scattering and e^+e^- or DM annihilations, we consider here. Eventually, one may ask how the size σ of the production region is connected to the parameter p_0 used in the conventional coalescence picture. Formally, we note that σ is approximately related to p_0 as $p_0/0.2\,\text{GeV} \sim 1\,\text{fm}/\sigma$. Note, however, that important physical inputs like the shape of the momentum distributions of antinucleons or the wave-function of the antideuteron affect p_0 and σ differently. Therefore such a relation has to be interpreted with care.

[2]The specified parameters correspond to the so-called φ_0-fit of the deuteron wave-function [13].

3 Determination of the spread σ

In order to test the validity of our coalescence model, i.e., in particular the universality of its parameter σ, we compare our predictions to experimental data on antideuteron production in e^+e^-, pp and pA collisions. Differences between the results of the standard and the new coalescence models were already investigated in Ref. [13], using as event generator PYTHIA. Here we focus instead on the new model, using the event generator QGSJET-II [24, 25], which reproduces experimental data over a wide energy range, for reactions involving nuclei as well as for pp collisions[3]. In addition, we employ PYTHIA 8.230 [28, 29] to simulate e^+e^- and DM annihilations as well as pp collisions. The considered experimental data sets are described in Appendix A. In Fig. 1, we show the best fits to the data on antideuteron production in pAl and pBe collisions at 200 GeV/c, while the fits to the transverse momentum p_T spectra of antideuterons in pp interactions, measured at CERN ISR and LHC, are plotted in Fig. 2. Because of the relatively large experimental uncertainties, the fits are in all cases acceptable. The corresponding fit results for the parameter σ obtained using QGSJET-II are listed in Table 1, while the results for PYTHIA are shown in Table 2. The values obtained for σ using PYTHIA have a smaller variance and are closer to the expected value of $\sigma \simeq 1$ fm, compared to the results for QGSJET-II.

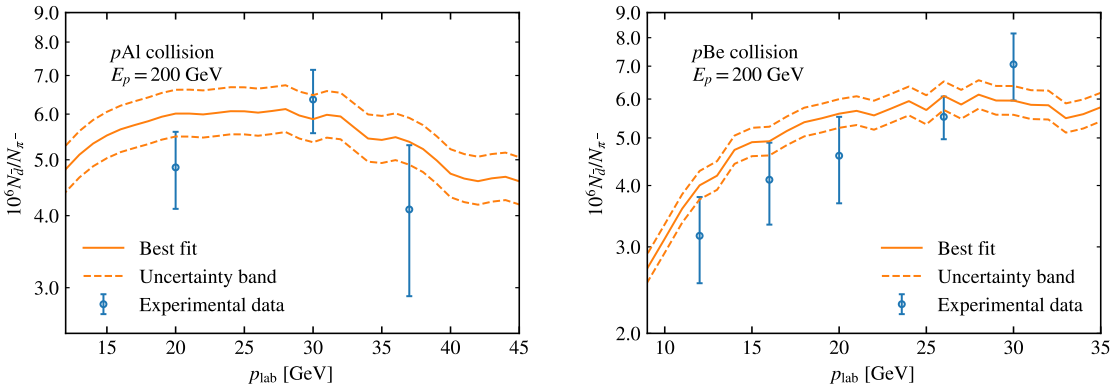

Figure 1. Best fit and 1σ uncertainty band for the antideuteron/pion ratio, obtained using QGSJET-IIm and the new coalescence model, for proton-aluminium (left) and proton-beryllium (right) collisions.

	LT ζ		const. ζ		standard coal.	
Experiment	σ [fm]	$\chi^2/(N-1)$	σ [fm]	$\chi^2/(N-1)$	p_0 [MeV]	$\chi^2/(N-1)$
p-p 7 TeV	1.44 ± 0.01	10/19	1.23 ± 0.01	86/19	134	93/19
p-p 2.76 TeV	1.29 ± 0.03	2.1/6	1.11 ± 0.02	9.9/6	146	12/6
p-p 900 GeV	1.02 ± 0.05	0.30/2	0.90 ± 0.04	0.68/2	175	0.88/2
p-p 53 GeV	0.50 ± 0.03	3.2/7	0.47 ± 0.03	2.9/7	280	2.5/7
p-Be	1.00 ± 0.03	2.2/4	0.95 ± 0.03	2.4/4	126	3.0/4
p-Al	0.88 ± 0.04	1.4/2	0.84 ± 0.04	1.5/2	126	1.3/2

Table 1. Calibration results for antideuteron production, obtained using QGSJET-II: including the effect of the Lorentz transformation on $\sigma_\perp$ [Eq. (2.3)], using constant $\sigma_\perp$, and employing the standard coalescence model.

[3] We are using a new tune of QGSJET-II-04m [26] which slightly improves the fit to the ALICE data [27] on antiproton production in pp collisions at $\sqrt{s} = 7$ TeV.

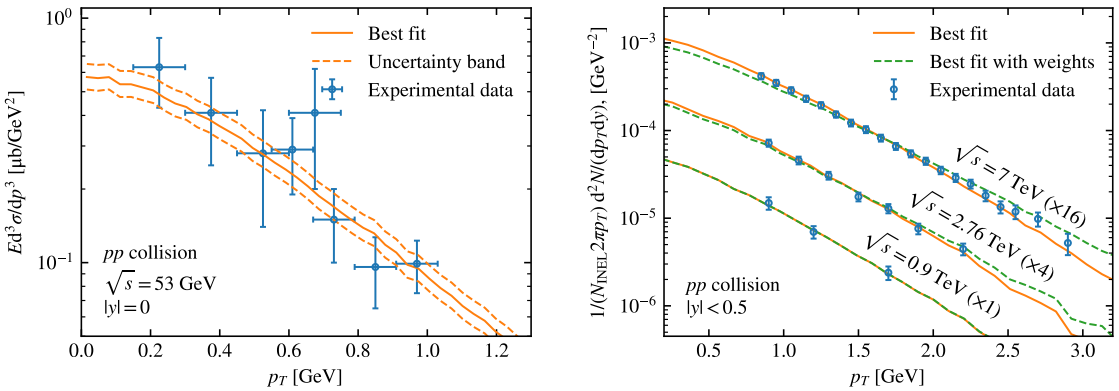

Figure 2. Best fit to antideuteron production data in pp collisions, using QGSJET-II and the new coalescence model. Left: results for $\sqrt{s} = 53$ GeV, including an uncertainty band, compared to CERN ISR data [20, 21]. Right: calculations for LHC energies, without and with the re-weighting to the pp data on antiproton production, as discussed in the text, compared to ALICE data [17].

	LT ζ		const. ζ		standard coal.	
Experiment	σ [fm]	$\chi^2/(N-1)$	σ [fm]	$\chi^2/(N-1)$	p_0 [MeV]	$\chi^2/(N-1)$
p-p 7 TeV	1.07 ± 0.01	29/19	0.92 ± 0.02	133/19	176	177/19
p-p 2.76 TeV	1.05 ± 0.02	8.7/6	0.93 ± 0.04	32/6	174	45.6/6
p-p 900 GeV	0.97 ± 0.05	2.6/2	0.87 ± 0.07	6.1/2	181	7.3/2
p-p 53 GeV	1.03 ± 0.06	3.3/7	0.96 ± 0.06	2.7/7	171	2.1/7
ALEPH	$1.04^{+0.20}_{-0.12}$	-	$0.99^{+0.18}_{-0.12}$	-	214^{+21}_{-26}	-
ALEPH+OPAL	$1.15^{+0.27}_{-0.22}$	3.2/1	$1.09^{+0.26}_{-0.22}$	3.2/1	201	3.2/1

Table 2. Calibration results for antideuteron production, obtained using PYTHIA 8.230.

Taking these results at face-value, one might interpret, e.g., the change from $\sigma \simeq 0.5$ fm at 53 GeV to $\sigma \simeq 1.44$ fm at 7 TeV, using QGSJET-II, as an energy dependence of this parameter. However, such a change may also be caused by a systematic bias either in the experimental data and/or in the predictions of the used event generators. In order to clarify the reason for this change, we compare in Fig. 3 the invariant differential yield of protons and antiprotons, measured by the ALICE collaboration [27, 30, 31], to the values obtained using QGSJET-II at $\sqrt{s} = 900$, 2760 and 7000 GeV, and using PYTHIA at $\sqrt{s} = 7000$ GeV. As is easily seen in the figure, QGSJET-II fits the data at 900 GeV well, but overestimates the bulk of the produced antiprotons at 2760 and 7000 GeV. Therefore, the coalescence parameter σ must be artificially increased at these energies to compensate the overproduction of antinucleons. In the same manner, QGSJET-II underestimates the antiproton flux measured at the CERN ISR[4]. Thus, σ has to be decreased for QGSJET-II to compensate this deviation. In all the aforementioned cases, the deviations from the expected value $\sigma \simeq 1$ fm are caused by an imperfect description of antiproton production by the Monte Carlo event generators.

In order to quantify this effect, we tweak the antiproton spectra by adding a weight $w = ap_T^b + c$ and fix a, b and c by fits to the experimental data. This implies that the weight $w_{\bar{d}} = [a(p_T/2)^b + c]^2$ has to be included in the case of antideuteron production. We fit the weight w to the combined antiproton and proton data measured by ALICE [27, 30, 31], with the same experimental set-up as the antideuteron data, and to the antiproton data measured at the CERN ISR[5] [33]. The resulting

[4] A short discussion of this effect on the standard coalescence model and CERN ISR data using PYTHIA and EPOS-LHC can be found in Ref. [32].

[5] In the fit of the CERN ISR data, $b = 1$ was fixed and only the data points in the interval $0.2 \leq p_T \leq 1.3$ GeV were

best-fit yields shown in Fig. 3 reproduce nicely the experimental data. Then we repeat the analysis of the antideuteron data of ALICE and CERN ISR: The values of σ obtained using the re-weighted antinucleon spectra are listed in Table 3 and the fits to the antideuteron data of ALICE are plotted in the right panel of Fig. 2. In all the cases, the results are significantly closer to the expected value $\sigma \simeq 1\,\mathrm{fm}$. Note that the weights are specific for each experimental set-up and kinematic range: They were chosen to affect mainly the shape of the antiproton spectra in the narrow kinematic range covered by experimental data. In contrast, the total yields important for astrophysical applications are less sensitive to the systematic uncertainties of the event generator at large p_T. For instance, the total antideuteron yield in pp collisions at 7 TeV, using $\sigma \simeq 1.1\,\mathrm{fm}$, would be decreased by $\simeq 40\%$, relative to the case of using no weights.

Finally, let us compare our results to those of Ref. [34]. Imposing the coalescence condition in momentum space on an event-by-event basis, the authors of that work used EPOS-LHC to reproduce experimental data on the (anti)deuteron yield in pp and pA collisions. Based on these comparisons, they suggested that p_0 is strongly energy dependent at low energies[6]. Moreover, they proposed that the energy dependence differs for deuteron and antideuteron production: While p_0 increases for deuterons, it decreases for antideuterons as the kinetic energy of the projectile decreases. Such a behaviour is difficult to understand, if one accepts that the strong interaction does not distinguish between matter and antimatter. In contrast, a possible contamination by deuterons produced in the detector may easily explain the larger value of p_0 for deuterons than for antideuterons. From a theoretical point of view, we expect that the size of the formation region—and thus σ—is only logarithmically dependent on the cm energy. Furthermore, its size should be identical for deuteron and antideuteron production. However, we have seen that a relatively small bias in the production spectra of antinucleons or, alternatively, systematic errors in the experimental results may delude an energy dependence of σ. Correcting for such biases, we have verified that the present experimental data are consistent with the universal coalescence picture implemented in our model. However, we note that the old data at $p_{\mathrm{lab}} = 70\,\mathrm{GeV}$ from Serpukhov [35] are inconsistent with this picture. A confirmation of these data could falsify the assumption underlying our model.

Based on the best fit values after re-weighting, we fix for the following analyses $\sigma = (1.0 \pm 0.1)\,\mathrm{fm}$ for both PYTHIA and QGSJET II. This value describes in our model via Eqs. (2.1–2.9) the formation of light antinuclei for all interaction types and energies. For comparisons, we set in the standard coalescence model $p_0 = 180\,\mathrm{MeV}$ for proton-proton, proton-nucleus and nucleus-nucleus collisions, while we use $p_0 = 210\,\mathrm{MeV}$ in DM annihilations.

	LT ζ		const. ζ		standard coal.	
Experiment	σ [fm]	$\chi^2/(N-1)$	σ [fm]	$\chi^2/(N-1)$	p_0 [MeV]	$\chi^2/(N-1)$
p-p 7 TeV	1.17 ± 0.01	19/19	0.97 ± 0.01	16.2/19	165	23/19
p-p 2.76 TeV	1.16 ± 0.02	3.6/6	0.99 ± 0.02	4.1/6	161	5.7/6
p-p 900 GeV	1.01 ± 0.05	0.30/2	0.89 ± 0.04	0.60/2	178	0.81/2
p-p 53 GeV	0.94 ± 0.06	2.7/7	0.89 ± 0.05	3.2/7	170	4.3/7

Table 3. Calibration results for antideuteron production in pp collisions, obtained by using QGSJET-II and applying an additional multiplicative weight $ap_T^b + c$ to the predicted antinucleon yield, as discussed in the text.

used.

[6] Note that their fit of p_0 as function of p_{lab} combines data from pp and pA collisions, which correspond to different cm energies. Moreover, the differences in the size of the formation region of deuterons as function of A are neglected in such an approach.

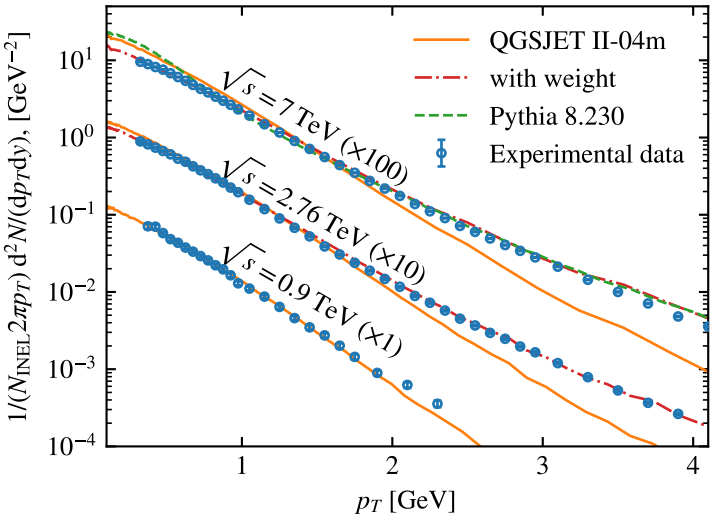

Figure 3. Combined invariant differential yield of protons and antiprotons in pp collisions, obtained using PYTHIA (green dashed line) and QGSJET-II (solid orange lines), compared to ALICE data [27, 30, 31]. The red dashed-dotted lines are obtained by adding a multiplicative weight $w = ap_T^b + c$ to the yield predicted by QGSJET-II.

4 Antinucleus source spectra

4.1 Secondary production

Light antinuclei are produced as secondaries in collisions of CRs with gas in the Galactic disc. We neglect elements heavier than helium but take into account the CR antiproton flux. The source term Q^{sec} of secondaries can then be written as

$$Q^{\mathrm{sec}}(T_{\bar{N}}, \boldsymbol{r}) = \sum_{i\in\{p,\mathrm{He},\bar{p}\}} \sum_{j\in\{p,\mathrm{He}\}} 4\pi n_j(\boldsymbol{r}) \int_{T^{(i,j)}_{\bar{N},\mathrm{min}}}^{\infty} \mathrm{d}T_i \, \frac{\mathrm{d}\sigma_{i,j}(T_i, T_{\bar{N}})}{\mathrm{d}T_{\bar{N}}} \Phi_i(T_i, \boldsymbol{r}), \tag{4.1}$$

where $n_j(\boldsymbol{r})$ is the density of particle j in the Galactic disc, $T = (E - m)/n$ is the kinetic energy per nucleon of the particle i with mass $m = nm_{\mathrm{N}}$ and flux Φ_i, while $T^{(i,j)}_{\bar{N},\mathrm{min}}$ is the threshold for creating an antinucleus $\bar{N}$. We use as hydrogen density $n_{\mathrm{H}} = 1\,\mathrm{cm}^{-3}$, while the helium density is fixed to $n_{\mathrm{He}} = 0.07 n_{\mathrm{H}}$. The differential cross section for $ij \to \bar{N}X$ is calculated as

$$\frac{\mathrm{d}\sigma_{i,j}(T_i, T_{\bar{N}})}{\mathrm{d}T_{\bar{N}}} = \sigma_{ij,\mathrm{inel}} \frac{\mathrm{d}N_{\bar{N}}(T_i, T_{\bar{N}})}{\mathrm{d}T_{\bar{N}}}, \tag{4.2}$$

where $\sigma_{ij,\mathrm{inel}}$ is the total inelastic cross section, while $\mathrm{d}N_{\bar{N}}(T_i, T_{\bar{N}})/\mathrm{d}T_{\bar{N}}$ is computed using our coalescence model. The parametrisations for the primary fluxes $\Phi_i(T_i, \boldsymbol{r})$ used in this work are compared to experimental data in Fig. 4. We will employ two parametrisations, one with and one without spectral breaks; their details are discussed in Appendix B.

We compute $\mathrm{d}\sigma_{ij}/\mathrm{d}T_{\bar{N}}$ for 100 logarithmically spaced energies E_i of the projectile up to 5×10^4 GeV for $i \in \{p, \mathrm{He}, \bar{p}\}$ and $j \in \{p, \mathrm{He}\}$. For each channel, we choose the lower end of the energy range for T_i such that all energies in which more than 10^{-9} antideuterons per event are produced are included. The contributions of all these processes, for different incoming energy ranges, are shown in Fig. 5. The differences caused by the breaks in the primary spectra are negligible below 10 GeV/n and small at higher energies; the largest difference appears for the contribution from primary helium. Furthermore, the difference between the new and standard coalescence models is small in pp and $\bar{p}p$ collisions, since the parameter p_0 is adjusted to reproduce the correct yield of antideuterons in

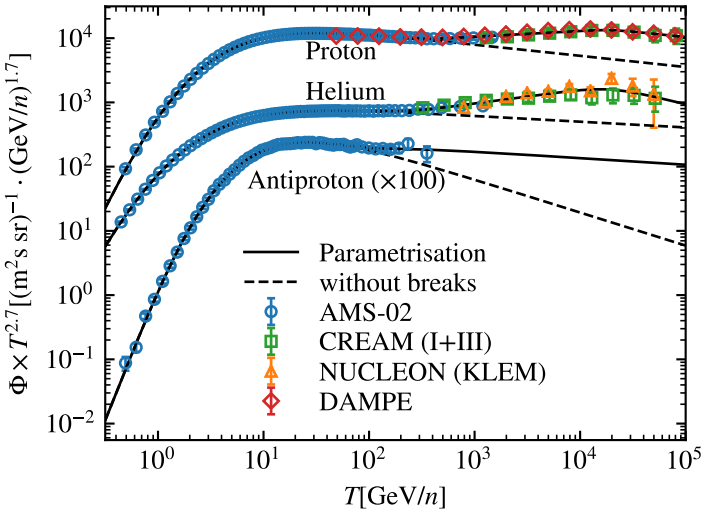

Figure 4. Parametrisations of the primary proton, helium and antiproton fluxes, compared to the data from AMS-02 [36–38], DAMPE [39] and CREAM [40].

pp collisions. However, the differences for the reactions involving helium are larger, up to a factor $\sim$ 2–3: While the new model takes into account the increase in the size of the formation region of antinucleons for helium, this effect is neglected in the case of the old coalescence model. Therefore the old treatment tends to over-predict the antideuteron yield in reactions involving helium.

The contributions of the different reactions to the total secondary source spectrum Q^{sec} of antideuterons are shown in Fig. 6. Our results can be compared to those of Lin *et al.* [41] and Ibarra and Wild [11]. Both groups used the standard coalescence model in a Monte Carlo approach: Lin *et al.* employed the event generators QGSJET-II-04m, EPOS-LHC and EPOS-1.99, while Ibarra and Wild used DPMJET-III and modified its results by adding a parametrised weight to the calculated antiproton spectra, in order to reproduce experimental data at low energies. We find that the main contribution to the secondary source term comes from pp collisions, as expected. However, the low energy part is dominated by pHe and HeHe interactions, which is a consequence of the kinematics of antideuteron production in these reactions, in particular, of their lower energy thresholds[7]: $T_{\bar{d},\mathrm{min}}^{(p,\mathrm{He})} = 10 m_N$ and $T_{\bar{d},\mathrm{min}}^{(\mathrm{He},\mathrm{He})} = 6 m_N$. These findings are in contrast to the results of both Lin *et al.* and Ibarra and Wild. Since both groups used the so-called nuclear enhancement factor ε, instead of performing a proper calculation of the antideuteron production in pHe, Hep and $\bar{p}$He collisions, they could not observe this low-energy behaviour. The limitations of the concept of a nuclear enhancement factor ε were studied in some detail in Refs. [26, 42]. In particular, the definition of ε assumes that the primary CR fluxes are power laws without breaks. Moreover, the nuclear enhancement factors for the production of massive particles are modified by threshold effects and are thus strongly energy dependent in the energy range relevant for astrophysical applications [26].

The contributions of different reaction types to the total secondary source term are shown in Fig. 6 for the new coalescence model and the broken primary spectra. The shaded area around the total contribution shown by the black solid line corresponds to the estimated model uncertainty obtained by varying σ in the range 0.9 to 1.1 fm. As one can see in Fig. 6, the "nuclear enhancement", i.e. the ratio of the values corresponding to the black[8] (total contribution) and blue (pp contribution) solid lines in the figure is indeed strongly energy-dependent. This applies, in particular, to the sub-GeV range where the partial contributions to the antideuteron source term from pHe and HeHe collisions

[7] In a proton-nucleus collision, $\bar{p}p$ and $\bar{n}n$ pairs may be produced by partial inelastic re-scatterings of the incident proton off two different target nucleons. In a nucleus-nucleus scattering, on the other hand, such pairs may be produced by partial inelastic interactions between two different pairs of the projectile and target nucleons.

[8] Modulo the small contributions from $\bar{p}p$ and $\bar{p}$He collisions.

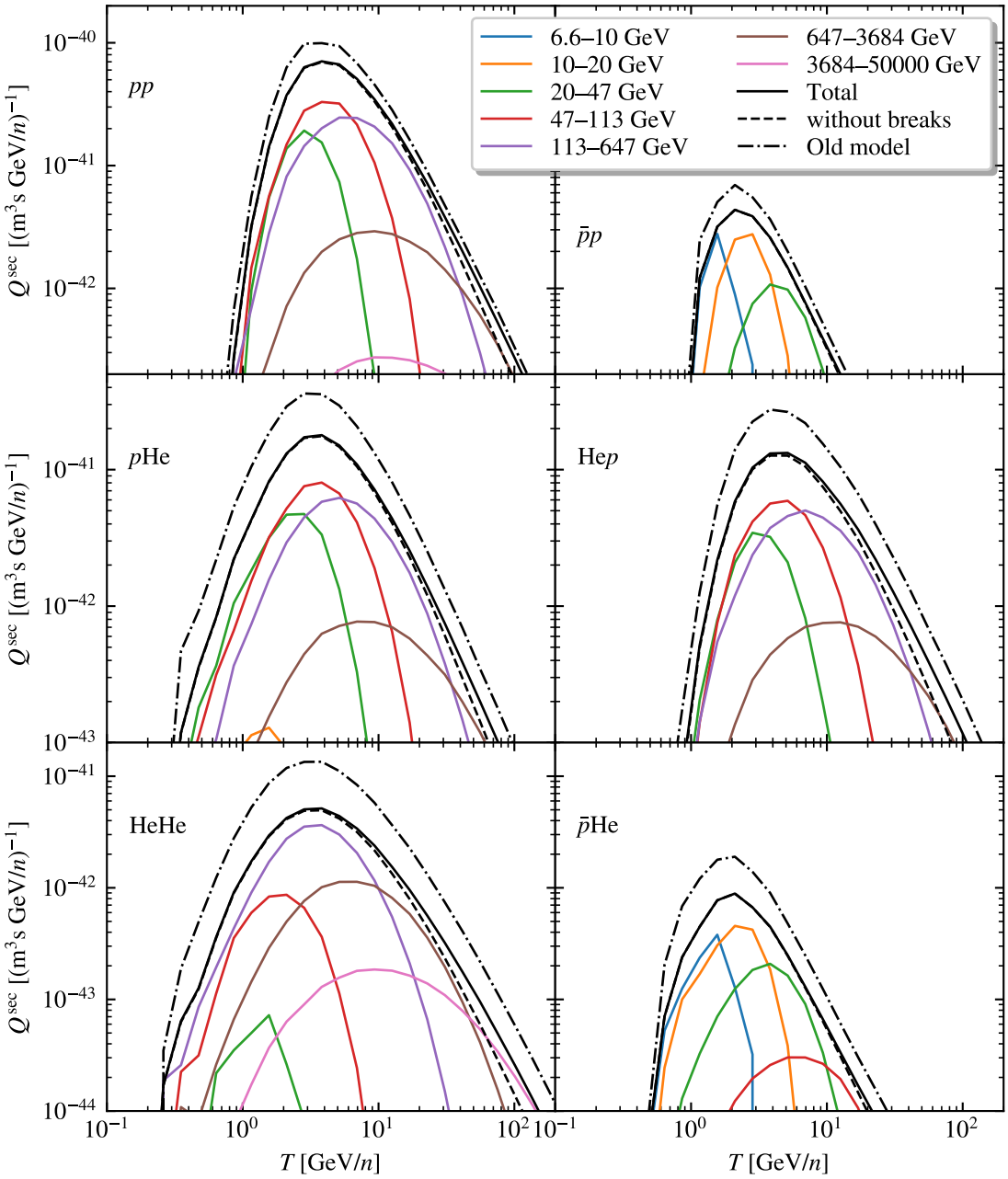

Figure 5. Partial contributions to the secondary source spectrum Q^{sec} of antideuterons for the six different reactions and from various energy ranges, for the new model and primary spectra with breaks. Additionally, the resulting total contributions (black solid lines) are compared to the ones obtained using the unbroken primary spectra (black dashed lines) and the old coalescence model (dashed-dotted black lines). The indicated energy ranges refer to the total energy per nucleon for the Hep contribution and to the total energy of the primary particle in all the other cases.

exceed the one from proton-proton scattering by orders of magnitude. The strong energy-dependence of the relative importance of the partial contributions to Q^{sec} at energies $T/n \lesssim 10\,\mathrm{GeV}$ is shown also clearly in Fig. 7. We conclude from this figure that the use of a nuclear enhancement factor at low

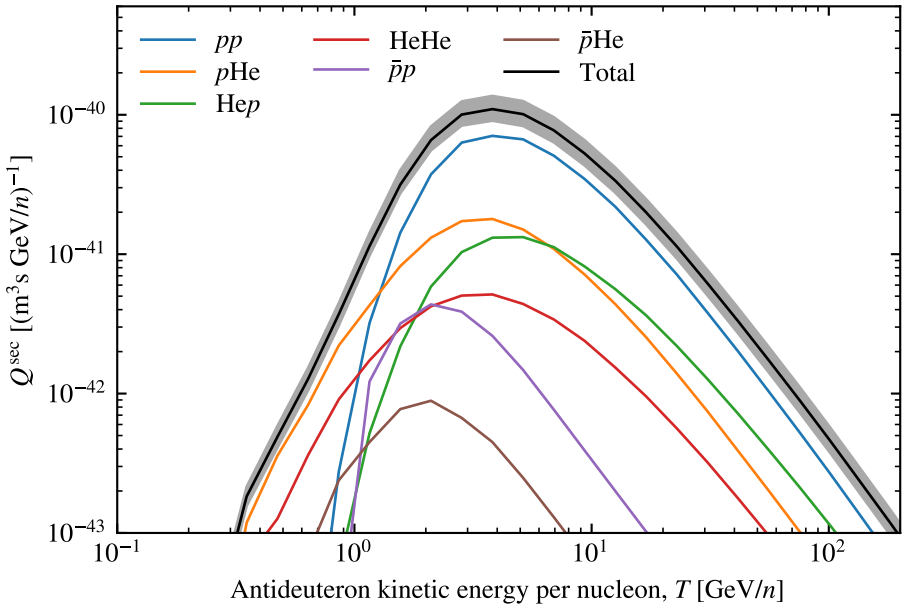

Figure 6. Contributions from different reaction types to the total secondary source term. The shaded area around the total corresponds to the estimated model uncertainty.

energies should be avoided.

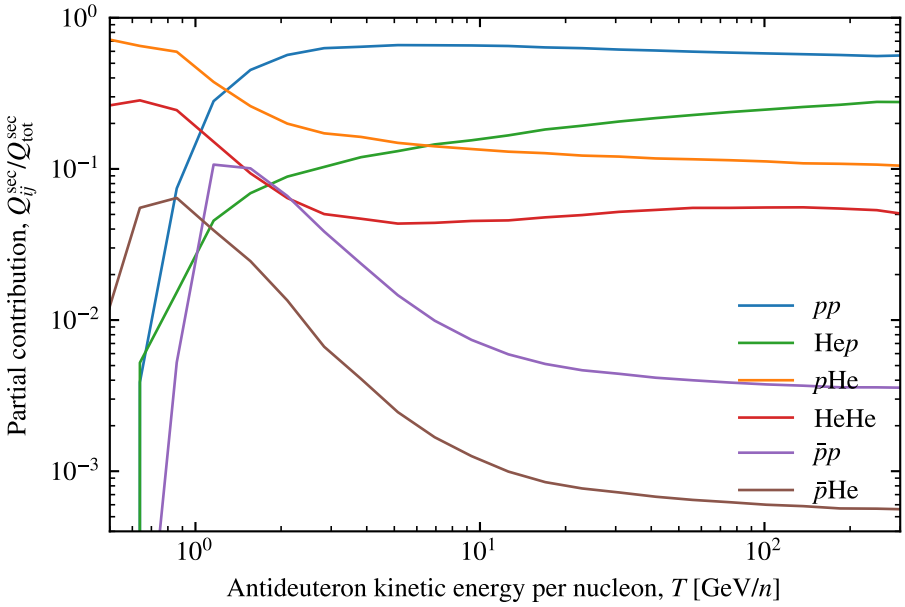

Figure 7. Relative contributions of the different reactions to the antideuteron source spectrum as function of kinetic energy per nucleon of the projectile.

Following the same procedure, we have calculated antihelium production in pp, pHe, Hep, HeHe, $\bar{p}p$ and $\bar{p}$He interactions, using 56 logarithmic bins from $E_p = 60$ to 5×10^3 GeV. The resulting contributions to the source spectrum are shown in Fig. 8 for different energy ranges of the primary

particles. The relative contributions from the various interactions are compared in Fig. 9. Since tritium decays fast compared to the propagation time scale, the plotted antihelium source spectrum includes also the antitritium contribution.

Comparing the source term of antihelium to the one of antideuteron, we see that its maximum is reduced by a factor few $\times 10^4$ and shifted somewhat to larger T/n. Otherwise, the same qualitative features discussed above for the antideuteron source term are still present. In particular, because of the possibility to interact with multiple target nucleons simultaneously, the contribution to the source term from pHe and HeHe collisions dominates the one from pp interactions up to few GeV/nucleon. There is also a notable difference concerning the relative contributions of $\bar{p}p$ and $\bar{p}$He collisions: As expected from threshold effects,[9] those are up to a factor ~ 10 smaller, compared to the antideuteron case, at $T/n \lesssim 50\,\mathrm{GeV}$. In any case, the contribution from $\bar{p}p$ interactions on the final antinuclei spectra is neglible.

4.2 Dark matter annihilations

In addition to the secondary production, we consider antinuclei originating from DM annihilations. We consider as DM particles Majorana fermions which annihilate purely into $\bar{b}b$ or W^+W^- pairs. These annihilations will be modelled in PYTHIA by generating a generic collision of a non-radiating e^+e^- pair with $\sqrt{s} = 2m_\chi$. The injection spectra $\mathrm{d}N/\mathrm{d}T$ are shown in Fig. 10 for antideuterons and in Fig. 11 for antihelium and antitritium. In both cases, we consider 100 and 1000 GeV as DM mass. Note that in the antideuteron injection spectra the differences between the standard and our new coalescence model can reach a factor of few, while they are much smaller in the spectra of antihelium-3. The reason for this mismatch are the wave-functions of the two nuclei: Since the one of the antideuteron is stronger peaked at $r = 0$ than the one of antihelium, large values of q in Eq. (2.1) are less suppressed for antideuterons, cf. with Fig. 4 of Ref. [13]. As a result, the differences in the shape of the antideuteron energy spectrum are more pronounced compared to the case of antihelium.

The DM source spectrum can be written as [43]

$$Q(\boldsymbol{r}, T) = \frac{1}{2}\frac{\rho^2(\boldsymbol{r})}{m_\chi^2}\,\langle\sigma_{\mathrm{ann}}v\rangle\,\frac{\mathrm{d}N^i_{\bar{N}}}{\mathrm{d}T_{\bar{N}}}, \tag{4.3}$$

where $\rho(\boldsymbol{r})$ is the DM mass density, m_χ its mass, $\langle\sigma_{\mathrm{ann}}v\rangle$ its thermally averaged annihilation cross section and $\mathrm{d}N_{\bar{N}}/\mathrm{d}T_{\bar{N}}$ is the differential number density of the antinuclei $\bar{N}$. An upper bound on $\langle\sigma_{\mathrm{ann}}v\rangle$ will be determined in Sec. 5.2, requiring that the antiproton flux measured by AMS-02 is not exceeded. The effect of different DM density profiles $\rho(\boldsymbol{r})$ is small compared to the propagation uncertainty and has already been extensively discussed, see e.g. Refs.[11, 44]. For simplicity, we will therefore only use an Einasto profile with $\alpha = 0.17$, $r_s = 28.4\,\mathrm{kpc}$ and $\rho_s = 0.033\,\mathrm{GeV/cm^3}$ [45].

5 Antinuclei fluxes

5.1 Propagation model

Charged particles diffuse in the turbulent Galactic magnetic field. We employ the two-zone diffusion model [46, 47] to describe the propagation of antinuclei through the Milky Way, which provides a simplistic but rather successful description of a variety of CR data. In this scheme, the Galaxy with radius $R = 20\,\mathrm{kpc}$ is modelled as a cylinder containing a large diffusive CR halo of half-height L and a thin disk of half-height $h \ll L$. The latter comprises the CR sources and the interstellar medium which serves as target for secondary production. In this model, the diffusion equation for the differential number density $n_{\bar{N}}$ of antinuclei can be written in cylindrical coordinates $\boldsymbol{r} = (r, z)$, where z is the height above the Galactic plane, as

$$\begin{aligned} -K\nabla^2 n_{\bar{N}} + \mathrm{sign}(z)V_c\partial_z n_{\bar{N}} + 2h\delta(z)\partial_E\left(b_{\mathrm{loss}}n_{\bar{N}} - D_{EE}\partial_E n_{\bar{N}}\right) \\ = Q^{\mathrm{prim}} + 2h\delta(z)\left[Q^{\mathrm{sec}} + Q^{\mathrm{ter}} - \Gamma_{\mathrm{ann}}n_{\bar{N}}\right], \end{aligned} \tag{5.1}$$

[9] Near threshold, an antideuteron is produced in the interactions $pp \to \bar{p}\bar{n}ppn$ and $\bar{p}p \to \bar{p}\bar{n}pn$, while an antihelium is produced in $pp \to \bar{p}\bar{p}\bar{n}pppn$ and $\bar{p}p \to \bar{p}\bar{p}\bar{n}ppn$. Thus, there is a larger relative change in going from antideuteron to antihelium in $\bar{p}p$ interactions than in pp.

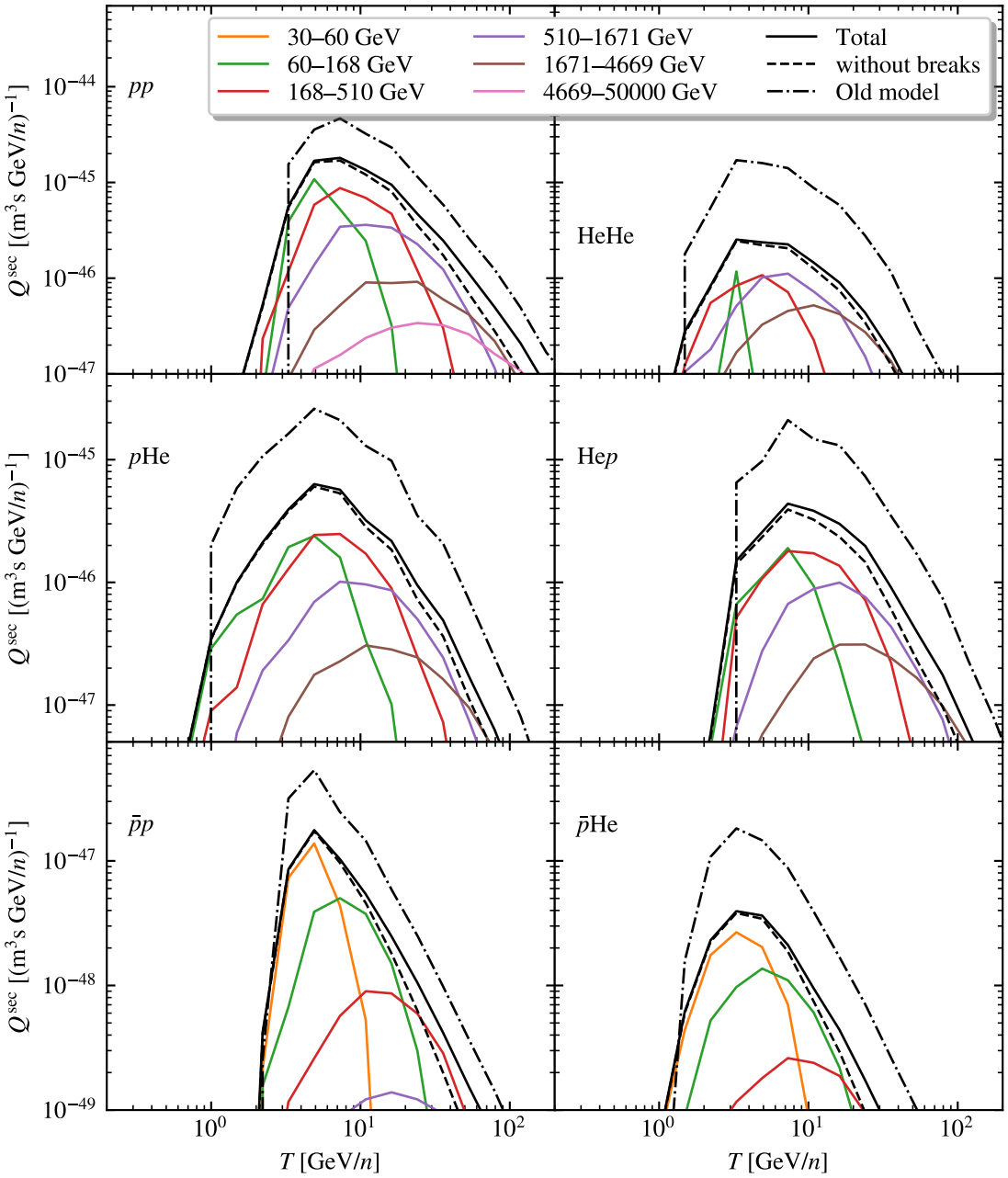

Figure 8. Partial contributions to the combined secondary source spectrum $Q^{\rm sec}$ of antihelium and antitritium, similar to Fig. 6.

where we have taken the limit $h = 100\,\mathrm{pc} \ll L$. We parametrise the rigidity-dependent diffusion coefficient as a simple power law,

$$K(\mathcal{R}) = \beta K_0 (\mathcal{R}/\mathrm{GV})^{\delta}, \tag{5.2}$$

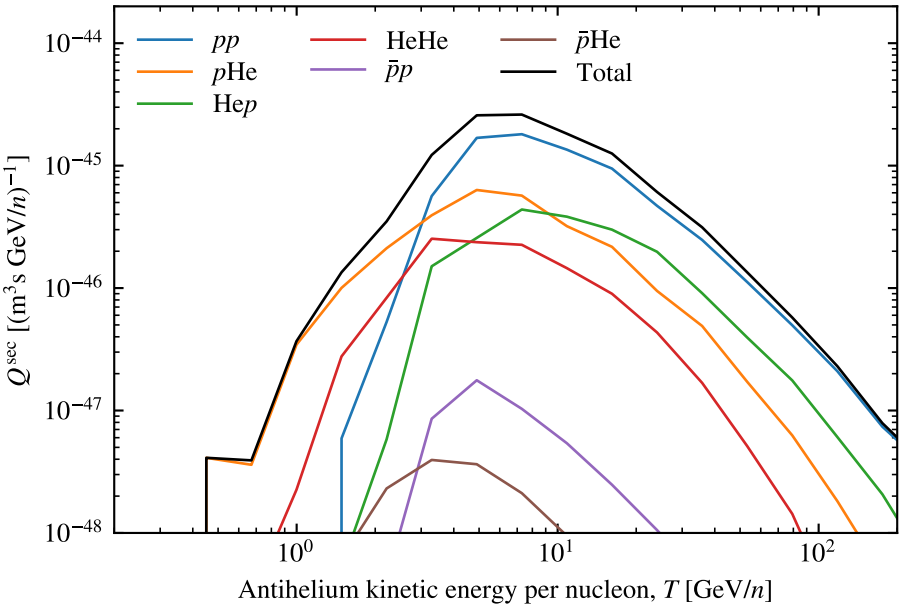

Figure 9. Contributions from different reaction types to the total secondary source term of antihelium.

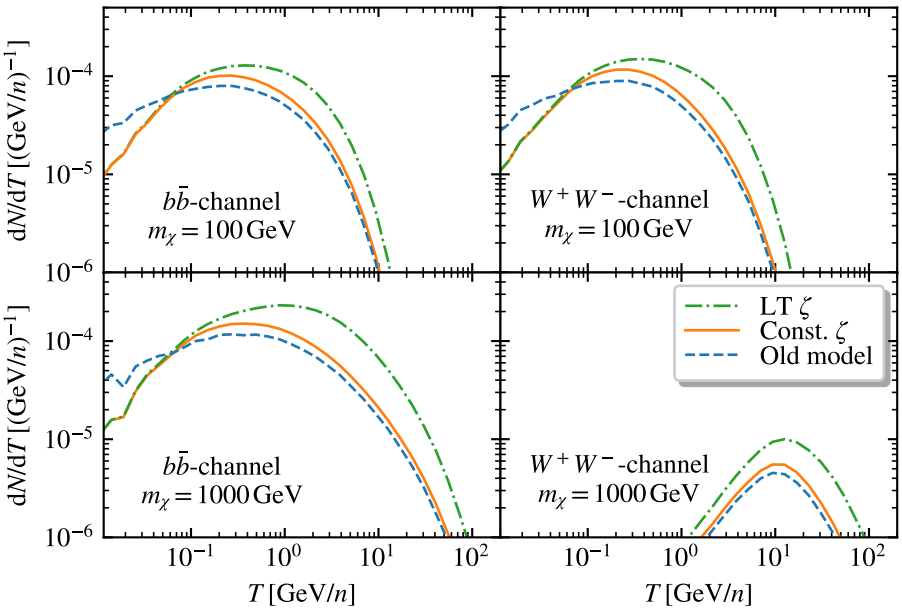

Figure 10. Antideuteron injection spectra from DM annihilations into $b\bar{b}$ (left) and W^+W^- (right), for $m_\chi = 100\,$GeV (top) and $m_\chi = 1000\,$GeV (bottom).

with $\mathcal{R} = E/(Ze)$, and K_0 and δ are free parameters. In turn, diffusion in momentum space, which is included as second-order re-acceleration in Eq. (5.1), is related to $K(\mathcal{R})$ by

$$D_{EE}(\mathcal{R}) = \frac{4}{3\delta(4-\delta^2)(4-\delta)} V_{\rm A}^2 \frac{v_{\bar{N}}^2 p_{\bar{N}}^2}{K(\mathcal{R})}\,, \tag{5.3}$$

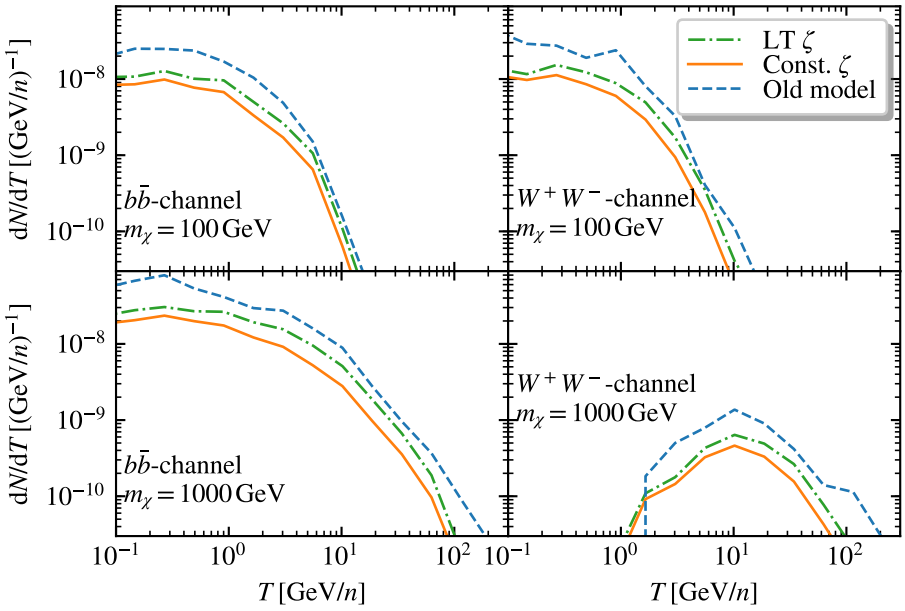

Figure 11. Antihelium (plus antitritium) injection spectra from DM annihilations into $b\bar{b}$ (left) and W^+W^- (right), for $m_\chi = 100\,\mathrm{GeV}$ (top) and $m_\chi = 1000\,\mathrm{GeV}$ (bottom).

where V_A is the Alfvén velocity, $v_{\bar{N}}$ is the velocity of the antinuclei and $p_{\bar{N}}$ their momentum. Moreover, V_c denotes the convection velocity which is assumed to be constant and directed away from the Galactic disc, while $\Gamma^{\bar{N}}_\mathrm{ann}$ is the annihilation rate of the antinuclei. The factor b_loss accounts for Coulomb, ionization and adiabatic energy losses. The primary proton, helium and antiproton fluxes are assumed to be the same in entire Galactic disc. The flux of antinuclei is related to the number density by $\Phi(E, \boldsymbol{r}) = v n_{\bar{N}}(E, \boldsymbol{r})/(4\pi)$.

The interaction rate of an antinucleus $\bar{N}$ will be approximated by $\Gamma_i^{\bar{N}p} = (n_\mathrm{H} + 4^{2/3} n_\mathrm{He}) v_{\bar{N}} \sigma^i_{\bar{N}p}$, where the factor $4^{2/3}$ accounts approximately for the cross section difference between helium and hydrogen, and $\sigma^\mathrm{ann}_{\bar{N}p}$ is the $\bar{N}p$ annihilation cross section. For antiprotons and antideuterons, we find the cross sections using the procedure discussed in Ref. [48], while for antihelium-3 we follow Ref. [49].

The tertiary term can be written as

$$Q^\mathrm{ter}(T_{\bar{N}}, \boldsymbol{r}) = 4\pi(n_\mathrm{H} + 4^{2/3} n_\mathrm{He}) \left[\int_{T_{\bar{N}}}^\infty \mathrm{d}T'_{\bar{N}} \, \frac{\mathrm{d}\sigma^\mathrm{non\text{-}ann}(\bar{N}(T'_{\bar{N}}) + p \to \bar{N}(T_{\bar{N}}) + X)}{\mathrm{d}T_{\bar{N}}} \Phi_{\bar{N}}(T'_{\bar{N}}, \boldsymbol{r}) \right.$$
$$\left. - \sigma^\mathrm{non\text{-}ann}(\bar{N}(T_{\bar{N}}) + p \to \bar{N}(T''_{\bar{N}}) + X) \Phi_{\bar{N}}(T_{\bar{N}}, \boldsymbol{r}) \right], \tag{5.4}$$

where $\Phi_{\bar{N}}(T_{\bar{N}}, \boldsymbol{r})$ is the antinucleus flux at energy $T_{\bar{N}}$. Thus, the tertiary terms are themselves dependent on the antinucleus flux and Eq. (5.1) becomes an integro-differential equation that we solve using the method presented in Ref. [50].

For antinuclei from WIMP annihilations, we neglect both re-acceleration and energy losses in Eq. (5.1), as they have been shown to have little impact on the final primary spectrum for $T \gtrsim 1\,\mathrm{GeV}$ [51]. We also neglect the tertiary contribution to the primary flux, since it is small for antiprotons and antideuterons because of their small non-annihilating inelastic cross section. For comparison, neglecting the tertiary contribution in the case of helium-3 leads to a flux that is roughly 40% lower compared to the opposite limit of neglecting the non-annihilating interactions [49]. In this case, one can use the common semi-analytical solution detailed, e.g., in Refs. [44, 45, 51]. Note,

Table 4. Parameters used for the two-zone propagation model.

Model	L [kpc]	δ	K_0 [kpc^2/Myr]	V_c [km/s]	V_A [km/s]
max	15	0.46	0.0765	5	117.6
med	4	0.7	0.0112	12	52.9
KRW	13.7	0.408	0.0967	0.2	31.9
Kolmogorov	5	1/3	0.018	0	0

however, that parts of the estimated sensitivities of the upcoming GAPS and AMS-02 experiments fall within the region $T \lesssim 1\,\mathrm{GeV}$ [52], which means that one should include the losses in a complete analysis of the low-energy range.

The final propagation model depends on five parameters: L, K_0, δ, V_c and V_A. In order to ease the comparison to earlier works, we employ the two parameter sets dubbed 'med' and 'max' in Ref. [53]. In addition, we use one parameter set inspired by a plain Kolmogorov diffusion model and the best-fit parameters from a recent B/C analysis [54] performed by Kappl[10] *et al.* For the former, we fix K_0 by requiring that the grammage $X = c\rho hL/(2K)$ crossed by CR protons with energy 10 GeV equals $10\,\mathrm{g/cm^2}$. The numerical values of the five parameters determining the propagation model are summarised in Table 4. Finally, we account for Solar modulations using the force-field approximation [55, 56] with a Fisk potential $\phi = 0.6\,\mathrm{GV}$, as described in Appendix B.

5.2 Upper bound on the annihilation cross section from AMS-02 antiproton data

The generic DM model used in this work has, apart from the branching ratios, two parameters: the DM mass m_χ and the thermally averaged annihilation cross section $\langle\sigma_{\mathrm{ann}}v\rangle$. We will here investigate the maximal flux of antinuclei consistent with the AMS-02 antiproton data [44]. There is currently no clear evidence for an exotic primary component in the antiproton spectrum and we use this absence to set an upper bound on the annihilation cross section for various DM masses. More precisely, we derive upper bounds on $\langle\sigma_{\mathrm{ann}}v\rangle$ by choosing as null-hypothesis the fit to the antiproton flux shown in Fig. 4. We then in turn vary the annihilation cross section until the χ^2 value differs by 3.84 from the null-hypothesis, corresponding to an 95% CL upper limit [57]. A stringent upper bound compatible with the antiproton flux is obtained when the same parameters are used in the antideuteron and antihelium cases. The results are shown in Fig. 12 for the considered parameter sets and the annihilation channels W^+W^- and $\bar{b}b$. The canonical value for a thermal relic, $\langle\sigma_{\mathrm{ann}}v\rangle = 3\times10^{-26}\,\mathrm{cm^3/s}$, and the upper bound obtained by the Fermi-LAT collaboration using dwarf galaxies [58] are plotted for comparison too. Note that the antiproton limits are more stringent than the recent Fermi-LAT bound. However, we stress that these limits only hold for the specific propagation model and astrophysical parameters used.

5.3 Detection prospects

The expected flux of light antinuclei at Earth from DM annihilations and secondary production can now be estimated by employing the two-zone propagation model and the force-field approximation, using the source spectra computed previously as input. For concreteness, we consider only the Einasto DM density profile. The antideuteron flux obtained with the new coalescence model, using the four sets of parameters for the diffusion model, is shown in Figs. 13 and 14. Additionally, we use the upper limit on the annihilation cross section imposed by the AMS-02 antiproton data as constraint. The shaded areas correspond to the expected sensitivity for the GAPS long duration balloon flight (105 days) (yellow) and 10-year data-taking of AMS-02 (purple) [10, 59, 60]. We find that the predicted antideuteron flux can be, for optimistic parameters, close to the sensitivity of these two experiments.

[10]Note that Kappl *et al.* used $n_{\mathrm{H}} = 0.9\,\mathrm{cm^{-3}}$ and $N_{\mathrm{He}} = 0.1\,\mathrm{cm^{-3}}$, meaning that our results are 9% higher as if we would use their parameter set.

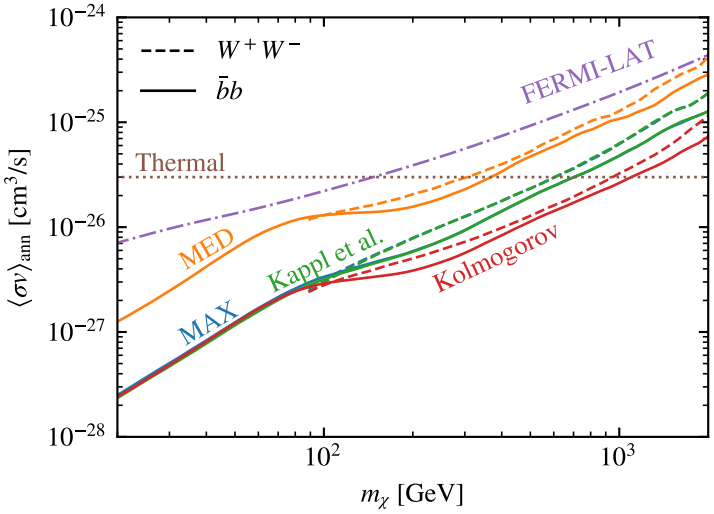

Figure 12. Upper limit compatible with the AMS-02 antiproton data for different propagation parameters. The upper limit from Fermi-LAT [58] (for $b\bar{b}$) and the value $\langle\sigma_{\rm ann}v\rangle$ favoured by cosmology are shown for comparison.

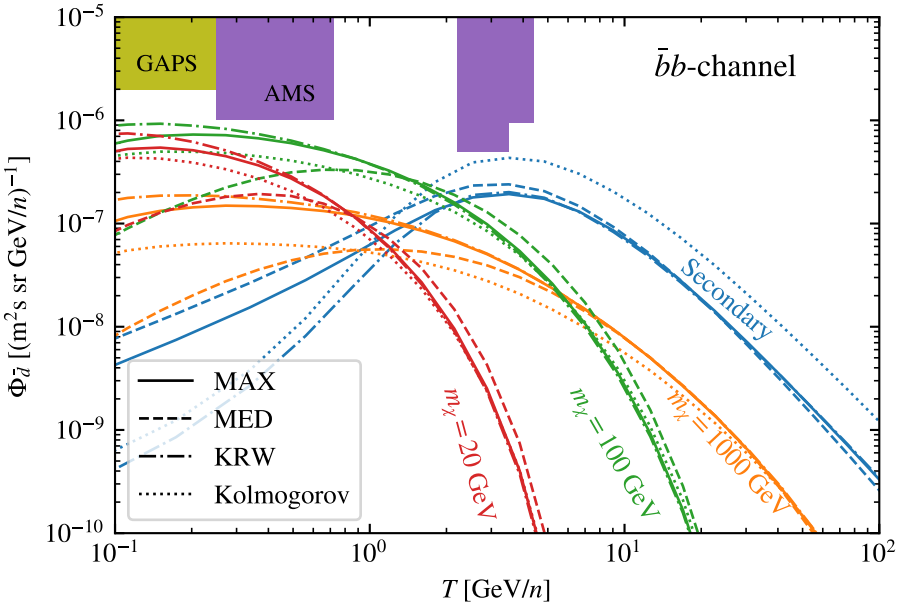

Figure 13. Estimated antideuteron flux on Earth from DM annihilations into $\bar{b}b$ pairs and from secondary production for the considered benchmark cases. The shaded areas on the top are the estimated AMS-02 and GAPS sensitivities.

The estimated antihelium-3 flux on Earth for the same benchmark cases as in the antideuteron case is shown in Fig. 15. The antihelium-3 sensitivity of AMS-02 is estimated by multiplying the 18-year $^3\bar{\rm He}$/He sensitivity from Ref. [61] with the helium flux measured by AMS-02 [37], and is further rescaled to the 10-year sensitivity. The better sensitivity for antihelium-3 than for antideuteron may

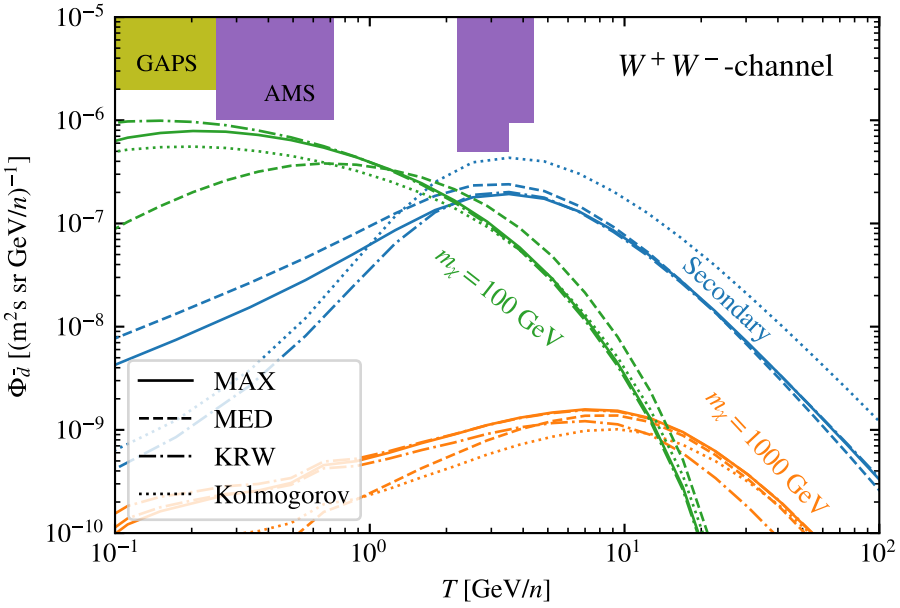

Figure 14. Estimated antideuteron flux on Earth from DM annihilations into W^+W^- pairs and from secondary production for the considered benchmark cases. The shaded areas on the top are the estimated AMS-02 and GAPS sensitivities.

explain why AMS-02 has reported eight antihelium candidates, while the number of antideuteron candidate events is still unknown. From Fig. 15, one can see that antihelium nuclei from secondary production are more likely to be detected than from DM annihilations.

There have been various other recent works investigating the detection prospects of antihelium-3 [2, 5, 49, 62–65]. The range of p_0 values used in these works varies considerably, depending e.g. on the data sets used for the calibration [2, 49, 64], the hadronisation model and the event generator [66, 67]. Since the yield of antinuclei scales as p_0^{3A-3}, a relatively modest increase of p_0 can boost the predictions towards the experimental sensitivities. Alternatively, it may be a promising avenue to investigate, if modified propagation models allow higher antideuteron and antihelium-3 fluxes, without being in a conflict with other observations. For instance, Ref. [65] proposed that strong re-acceleration can increase the number of expected antideuteron and antihelium-3 events considerably.

6 Summary and conclusions

The coalescence momentum p_0 of the usually employed coalescence models in momentum space is a free parameter that must be fitted to experimental data. Although p_0 should be independent on both the center-of-mass energy of the collision and the reaction type, the value obtained by fitting the model to data from different reactions varies considerably [10–12, 34]. In contrast, we have shown that the single parameter σ of our alternative coalescence model is universal, agreeing numerically well with its interpretation as the size of the formation region of antinuclei. Therefore, the production of antideuteron and antihelium-3 can be described successfully both for point-like interactions (e^+e^-, DM decays and annihilations) and for hadronic and nuclear interactions, using a single free parameter.

Combining our coalescence model with the event generator QGSJET-II-04m, we have calculated consistently the yield of antideuterons in proton-proton, proton-helium, helium-helium, antiproton-proton and antiproton-helium collisions. Thereby we avoided the use of a nuclear enhancement factor, which is generally ill-defined [26, 42]. In particular, we found that the low energy tail of the secondary source spectrum of antinuclei is strongly dominated by the contributions of proton-helium and helium-

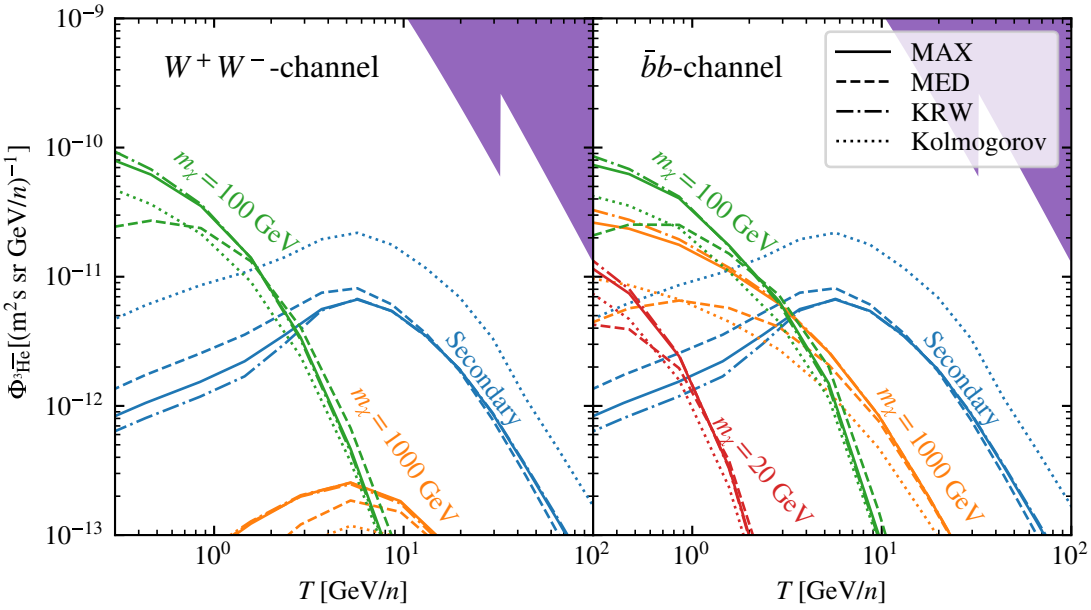

Figure 15. Estimated antihelium-3 flux on Earth from WIMP annihilations and secondary production for the considered benchmark cases and the considered propagation parameters. The shaded area on the top right is the estimated 10-year AMS-02 sensitivity.

helium collisions. This is in contrast to previous works using a nuclear enhancement factor, which found that antiproton collisions should be dominant due to the low threshold energy. Moreover, our new coalescence model takes into account the increase of the size of the formation region of antinuclei in reactions involving helium, an effect which is neglected using the old coalescence model. Therefore the old treatment tends to over-predict the antideuteron yield in reactions involving helium.

Using a two-zone diffusion model, we derived the resulting fluxes of antideuterons and antihelium. Our results indicate that no antihelium nuclei from secondary production or from WIMP annihilations should be detected during 10-years of operation of AMS-02 and the long duration balloon flights of GAPS. In contrast, the antideuteron flux can be close to the sensitivities of the AMS-02 and GAPS experiments. Since our analysis contains several sources of uncertainties related to, e.g. the propagation model, nuclear cross sections, and the coalescence model, the true fluxes might be well higher and thus in reach of these experiments. We note also that updated sensitivity analyses for both antideuteron and antihelium are highly warranted. The GAPS experiment is most sensitive to low-energy antideuterons from light DM. In that energy range, a more complete numerical treatment of the CR propagation would be desirable. In the case of antihelium-3, the contribution from CR interaction on gas is closer to the expected sensitivity than from DM annihilations. An interesting avenue to investigate is whether modified propagation models allow higher antihelium-3 fluxes without being in a conflict with other observations.

Acknowledgements

S.O. acknowledges support from the project OS 481/2-1 of the Deutsche Forschungsgemeinschaft.

A Experimental data used

We only consider experiments on antideuteron production, i.e., we neglect the experimental data on deuteron production. In this way, we avoid possible contaminations from the production of deuterons

in the detector material.

A.1 e^+e^- annihilations

The ALEPH [15] and OPAL collaboration [16] at LEP measured the deuteron and the antideuteron fluxes in e^+e^- collisions at the Z resonance. The ALEPH collaboration measured a production of $(5.9 \pm 1.8 \pm 0.5) \times 10^{-6}$ antideuterons per hadronic Z decay in the antideuteron momentum range $0.62 < p < 1.03\,\mathrm{GeV}$ and a production angle $|\cos\vartheta| < 0.95$. Here, the first uncertainty is the statistical and the second one is the systematic error. In contrast, the OPAL collaboration did not detect any antideuterons in the momentum range $0.35 < p < 1.1\,\mathrm{GeV}$. We take the resulting upper limit into account by following the procedure discussed in Ref. [12].

A.2 Proton-proton collisions

The ALICE collaboration measured the invariant differential yield $E\,\mathrm{d}^3n/\mathrm{d}p^3$ of antideuterons, antitritium and antihelium-3 in inelastic proton-proton collisions at centre of mass energies $\sqrt{s} = \{0.9, 2.76, 7\}\,\mathrm{TeV}$ in the p_T range $0.8\,\mathrm{GeV} < p_T < 3\,\mathrm{GeV}$ and rapidity range $|y| < 0.5$ [17]. The experiment included a trigger (V0) that required a hit (charged particle) in both of the two pseudo-rapidity ranges $2.8 < \eta < 5.1$ and $-3.7 < \eta < -1.7$, used to select non-diffractive inelastic events. We generate inelastic events and only include those which satisfy the V0 trigger.

The inclusive differential cross section of antideuterons at $\vartheta_{\mathrm{cm}} = 90°$ ($y = 0$) in $\sqrt{s} = 53\,\mathrm{GeV}$ pp collisions was measured at CERN ISR [20, 21]. We compute the differential cross section as $E\,\mathrm{d}^3\sigma/\mathrm{d}p^3 = \sigma_{\mathrm{inel}}/(2\pi p_T N_{\mathrm{inel}})(\mathrm{d}^2N/\mathrm{d}p_T\,\mathrm{d}y)$ and require that $|y| < 0.1$.

A.3 Proton-beryllium and proton-aluminium collisions

The production of d, t, ^{3}He, $\bar{d}$, $\bar{t}$ and $^3\bar{\mathrm{He}}$ at 0° with momenta between 12 and 37 GeV in the lab frame in p-beryllium and p-aluminium collisions at $200\,\mathrm{GeV}/c$ was reported in Ref. [19]. The results are presented as ratios of antinuclei and π^- yields. The antideuteron results had been split into three and five bins between 20 and 37 GeV in p-aluminium and p-beryllium collisions, respectively. As the data are given for 0° in the lab frame, and we are only interested in the bulk of produced antinuclei, we include all produced π^- and antideuterons in the analysis.

B Parametrisation of the primary cosmic ray flux

In order to describe the secondary production of antinuclei, one needs the primary fluxes of protons, helium and antiprotons as input. The primary CR fluxes were traditionally parametrised by an unbroken power law up to the CR knee, as $\Phi(T) \propto T^{-\gamma}$, where T is the kinetic energy of the particle and $\gamma \sim 2.7$. However, recent experimental data, such as from the AMS-02 [36–38] and CREAM [40] experiments, clearly suggest that there is a hardening in the CR flux around the rigidity $\mathcal{R} \sim 400\,\mathrm{GeV}$. In addition, there are now several experiments, including CREAM and DAMPE [39], suggesting that there is an additional break around 10 TeV. For a spectrum with N statistical significant breaks, we fit the function

$$\Phi(T) = AT^{-\gamma}\left(\frac{T}{T+b}\right)^c \prod_{i=1}^{N} f(T_{\mathrm{b}i}, \Delta\gamma_i, s), \tag{B.1}$$

where

$$f(T_{\mathrm{b}}, \Delta\gamma, s) = \left[1 + \left(\frac{T}{T_{\mathrm{b}}}\right)^s\right]^{\Delta\gamma/s} \tag{B.2}$$

accounts for the breaks, while the first parentheses is included to reproduce the low energy part of the spectra. We follow Ref. [39] and fix the smoothness parameter $s = 5$ for proton and antiproton, while we find that $s = 3$ provides a good fit for helium. The parameters $\Delta\gamma_i$ describe the changes in the power-law index. Thus, for each additional break, we add two free parameters, while for the main spectrum, we have four free parameters. We fix the parameters by first fitting

$$\Phi_{\text{AMS-02}}(T) = AT^{-\gamma}\left(\frac{T}{T+b}\right)^c, \tag{B.3}$$

	A [m^{2}s sr /(GeV/n)]	b [GeV/n]	c	γ	$T_{\rm b1}$ [GeV/n]	$\Delta\gamma_1$	$T_{\rm b2}$ [GeV/n]	$\Delta\gamma_2$	χ^2/d.f.
Proton	26714	0.49	6.81	2.88	343	0.265	19503	-0.264	0.39
Helium	1151	1.06	2.74	2.79	237	0.309	18849	-0.620	0.95
Antiproton	22.4	1.28	9.22	3.22	88.4	0.412			0.39

Table 5. Parameters for the fits of the primary proton, helium, and antiproton spectra at local interstellar space. The fitting procedure is discussed in the text.

to the AMS-02 proton data up to the hardening at $T \sim 400\,\mathrm{GeV}/n$ and in turn fix the remaining parameters by using Eq. (B.1).

We take into account solar modulation by using the force field approximation [55]. Based on the Oulu NM database [68], we find the mean solar modulation force-field ϕ in the periods of data taking [69, 70]. Since solar modulation can be neglected at high energies, this is only relevant for the AMS-02 data. For the proton and helium fluxes, we obtained $\phi = 0.60\,\mathrm{GV}$, while we found $\phi = 0.62\,\mathrm{GV}$ for the antiproton flux. Our fit results are listed in Table 5.

References

[1] F. Donato, N. Fornengo and P. Salati, *Anti-deuterons as a signature of supersymmetric dark matter*, *Phys. Rev.* **D62** (2000) 043003 [hep-ph/9904481].

[2] M. Cirelli, N. Fornengo, M. Taoso and A. Vittino, *Anti-helium from dark matter annihilations*, *JHEP* **08** (2014) 009 [1401.4017].

[3] P. von Doetinchem et al., *Cosmic-ray Antinuclei as Messengers of New Physics: Status and Outlook for the New Decade*, 2002.04163.

[4] P. Chardonnet, J. Orloff and P. Salati, *The production of antimatter in our galaxy*, *Phys. Lett.* **B409** (1997) 313 [astro-ph/9705110].

[5] V. Poulin, P. Salati, I. Cholis, M. Kamionkowski and J. Silk, *Where do the AMS-02 antihelium events come from?*, *Phys. Rev.* **D99** (2019) 023016 [1808.08961].

[6] A. Schwarzschild and C. Zupancic, *Production of Tritons, Deuterons, Nucleons, and Mesons by 30-GeV Protons on A-1, Be, and Fe Targets*, *Phys. Rev.* **129** (1963) 854.

[7] S. T. Butler and C. A. Pearson, *Deuterons from high-energy proton bombardment of matter*, *Phys. Rev.* **129** (1963) 836.

[8] M. Kadastik, M. Raidal and A. Strumia, *Enhanced anti-deuteron dark matter signal and the implications of PAMELA*, *Phys. Lett.* **B683** (2010) 248 [0908.1578].

[9] L. A. Dal, *Antideuterons as signature for dark matter*, master's thesis, NTNU Trondheim, available at http://hdl.handle.net/11250/246403, 2011.

[10] T. Aramaki et al., *Review of the theoretical and experimental status of dark matter identification with cosmic-ray antideuterons*, *Phys. Rept.* **618** (2016) 1 [1505.07785].

[11] A. Ibarra and S. Wild, *Prospects of antideuteron detection from dark matter annihilations or decays at AMS-02 and GAPS*, *JCAP* **1302** (2013) 021 [1209.5539].

[12] L. A. Dal and A. R. Raklev, *Alternative formation model for antideuterons from dark matter*, *Phys. Rev.* **D91** (2015) 123536 [1504.07242].

[13] M. Kachelrieß, S. Ostapchenko and J. Tjemsland, *Alternative coalescence model for deuteron, tritium, helium-3 and their antinuclei*, *Eur. Phys. J.* **A56** (2020) 4 [1905.01192].

[14] R. Scheibl and U. W. Heinz, *Coalescence and flow in ultrarelativistic heavy ion collisions*, *Phys. Rev.* **C59** (1999) 1585 [nucl-th/9809092].

[15] ALEPH collaboration, *Deuteron and anti-deuteron production in e+ e- collisions at the Z resonance*, *Phys. Lett.* **B639** (2006) 192 [hep-ex/0604023].

[16] OPAL collaboration, *Search for heavy charged particles and for particles with anomalous charge in e^+e^- collisions at LEP*, *Z. Phys.* **C67** (1995) 203.

[17] ALICE collaboration, *Production of deuterons, tritons, ^{3}He nuclei and their antinuclei in pp collisions at $\sqrt{s}$ = 0.9, 2.76 and 7 TeV*, *Phys. Rev.* **C97** (2018) 024615 [1709.08522].

[18] A. Bussière, G. Giacomelli, E. Lesquoy, R. Meunier, L. Moscoso, A. Müller et al., *Particle Production and Search for Longlived Particles in 200-GeV/c to 240-GeV/c Proton - Nucleon Collisions*, *Nucl. Phys.* **B174** (1980) 1.

[19] W. Bozzoli, A. Bussière, G. Giacomelli, E. Lesquoy, R. Meunier, L. Moscoso et al., *Search for Longlived Particles in 200-GeV/c Proton - Nucleon Collisions*, *Nucl. Phys.* **B159** (1979) 363.

[20] B. Alper et al., *Large angle production of stable particles heavier than the proton and a search for quarks at the CERN Intersecting Storage Rings*, *Phys. Lett.* **46B** (1973) 265.

[21] British-Scandinavian-MIT collaboration, *Production of Deuterons and anti-Deuterons in Proton Proton Collisions at the CERN ISR*, *Lett. Nuovo Cim.* **21** (1978) 189.

[22] T. W. Donnelly, J. A. Formaggio, B. R. Holstein, R. G. Milner and B. Surrow, *Foundations of Nuclear and Particle Physics*. Cambridge University Press, 2017.

[23] K. Blum and M. Takimoto, *Nuclear coalescence from correlation functions*, *Phys. Rev.* **C99** (2019) 044913 [1901.07088].

[24] S. Ostapchenko, *Monte Carlo treatment of hadronic interactions in enhanced Pomeron scheme: I. QGSJET-II model*, *Phys. Rev.* **D83** (2011) 014018 [1010.1869].

[25] S. Ostapchenko, *QGSJET-II: physics, recent improvements, and results for air showers*, *EPJ Web Conf.* **52** (2013) 02001.

[26] M. Kachelrieß, I. V. Moskalenko and S. S. Ostapchenko, *New calculation of antiproton production by cosmic ray protons and nuclei*, *Astrophys. J.* **803** (2015) 54 [1502.04158].

[27] ALICE collaboration, *Measurement of pion, kaon and proton production in proton–proton collisions at $\sqrt{s} = 7$ TeV*, *Eur. Phys. J.* **C75** (2015) 226 [1504.00024].

[28] T. Sjöstrand, S. Mrenna and P. Z. Skands, *PYTHIA 6.4 Physics and Manual*, *JHEP* **05** (2006) 026 [hep-ph/0603175].

[29] T. Sjöstrand, S. Ask, J. R. Christiansen, R. Corke, N. Desai, P. Ilten et al., *An Introduction to PYTHIA 8.2*, *Comput. Phys. Commun.* **191** (2015) 159 [1410.3012].

[30] ALICE collaboration, *Production of pions, kaons and protons in pp collisions at $\sqrt{s} = 900$ GeV with ALICE at the LHC*, *Eur. Phys. J.* **C71** (2011) 1655 [1101.4110].

[31] ALICE collaboration, *Production of charged pions, kaons and protons at large transverse momenta in pp and Pb–Pb collisions at $\sqrt{s_{\rm NN}}$ =2.76 TeV*, *Phys. Lett.* **B736** (2014) 196 [1401.1250].

[32] ALICE collaboration, *Supplemental material: Afterburner for generating light (anti-)nuclei with QCD-inspired event generators in pp collisions*, *ALICE-PUBLIC-2017-010* (2017) .

[33] British-Scandinavian collaboration, *Production Spectra of pi+-, K+-, rho+- at Large Angles in Proton Proton Collisions in the CERN Intersecting Storage Rings*, *Nucl. Phys.* **B100** (1975) 237.

[34] D.-M. Gomez-Coral, A. Menchaca Rocha, V. Grabski, A. Datta, P. von Doetinchem and A. Shukla, *Deuteron and Antideuteron Production Simulation in Cosmic-Ray Interactions*, *Phys. Rev.* **D98** (2018) 023012 [1806.09303].

[35] V. V. Abramov et al., *High p_T Deuteron and Anti-deuteron Production in pp and p a Collisions at 70-GeV*, *Sov. J. Nucl. Phys.* **45** (1987) 845.

[36] AMS collaboration, *Precision Measurement of the Proton Flux in Primary Cosmic Rays from Rigidity 1 GV to 1.8 TV with the Alpha Magnetic Spectrometer on the International Space Station*, *Phys. Rev. Lett.* **114** (2015) 171103.

[37] AMS collaboration, *Precision Measurement of the Helium Flux in Primary Cosmic Rays of Rigidities*

1.9 GV to 3 TV with the Alpha Magnetic Spectrometer on the International Space Station, *Phys. Rev. Lett.* **115** (2015) 211101.

[38] AMS collaboration, *Antiproton Flux, Antiproton-to-Proton Flux Ratio, and Properties of Elementary Particle Fluxes in Primary Cosmic Rays Measured with the Alpha Magnetic Spectrometer on the International Space Station*, *Phys. Rev. Lett.* **117** (2016) 091103.

[39] DAMPE collaboration, *Measurement of the cosmic-ray proton spectrum from 40 GeV to 100 TeV with the DAMPE satellite*, *Sci. Adv.* **5** (2019) eaax3793 [1909.12860].

[40] Y. S. Yoon et al., *Proton and Helium Spectra from the CREAM-III Flight*, *Astrophys. J.* **839** (2017) 5 [1704.02512].

[41] S.-J. Lin, X.-J. Bi and P.-F. Yin, *Expectations of the Cosmic Antideuteron Flux*, 1801.00997.

[42] M. Kachelrieß, I. V. Moskalenko and S. S. Ostapchenko, *Nuclear enhancement of the photon yield in cosmic ray interactions*, *Astrophys. J.* **789** (2014) 136 [1406.0035].

[43] G. Jungman, M. Kamionkowski and K. Griest, *Supersymmetric dark matter*, *Phys. Rept.* **267** (1996) 195 [hep-ph/9506380].

[44] N. Fornengo, L. Maccione and A. Vittino, *Dark matter searches with cosmic antideuterons: status and perspectives*, *JCAP* **1309** (2013) 031 [1306.4171].

[45] M. Cirelli, G. Corcella, A. Hektor, G. Hutsi, M. Kadastik, P. Panci et al., *PPPC 4 DM ID: A Poor Particle Physicist Cookbook for Dark Matter Indirect Detection*, *JCAP* **1103** (2011) 051 [1012.4515].

[46] V. L. Ginzburg and S. I. Syrovatskii, *The origin of cosmic rays*. New York: Gordon and Breach, 1969.

[47] V. L. Ginzburg, I. M. Khazan and V. S. Ptuskin, *Origin of Cosmic-Rays - Galactic Models with Halo - Part One - Proton Nucleon Component*, *Astrophys. Space Sci.* **68** (1980) 295.

[48] T. Delahaye and M. Grefe, *Antideuterons from Decaying Gravitino Dark Matter*, *JCAP* **1507** (2015) 012 [1503.01101].

[49] E. Carlson, A. Coogan, T. Linden, S. Profumo, A. Ibarra and S. Wild, *Antihelium from dark matter*, *Phys. Rev.* **D89** (2014) 076005 [1401.2461].

[50] F. Donato, D. Maurin, P. Salati, A. Barrau, G. Boudoul and R. Taillet, *Anti-protons from spallations of cosmic rays on interstellar matter*, *Astrophys. J.* **563** (2001) 172 [astro-ph/0103150].

[51] D. Maurin, R. Taillet and C. Combet, *Approximate formulae for exotic GCR anti-protons and anti-deuterons: Fluxes and astrophysical uncertainties*, *arXiv e-prints* (2006) [astro-ph/0609522].

[52] GAPS collaboration, *Antideuteron Sensitivity for the GAPS Experiment*, *Astropart. Phys.* **74** (2016) 6 [1506.02513].

[53] F. Donato, N. Fornengo and D. Maurin, *Antideuteron fluxes from dark matter annihilation in diffusion models*, *Phys. Rev.* **D78** (2008) 043506 [0803.2640].

[54] R. Kappl, A. Reinert and M. W. Winkler, *AMS-02 Antiprotons Reloaded*, *JCAP* **1510** (2015) 034 [1506.04145].

[55] L. J. Gleeson and W. I. Axford, *Solar Modulation of Galactic Cosmic Rays*, *Astrophys. J.* **154** (1968) 1011.

[56] H. Moraal, *Cosmic-Ray Modulation Equations*, *Space Sci. Rev.* **176** (2013) 299.

[57] C. Patrignani et al., *Review of Particle Physics*, *Chin. Phys.* **C40** (2016) 100001.

[58] Fermi-LAT collaboration, *Searching for Dark Matter Annihilation from Milky Way Dwarf Spheroidal Galaxies with Six Years of Fermi Large Area Telescope Data*, *Phys. Rev. Lett.* **115** (2015) 231301 [1503.02641].

[59] AMS-02 collaboration, *Cosmic Rays Antideuteron Sensitivity for AMS-02 Experiment*, in *Proceedings, 30th International Cosmic Ray Conference (ICRC 2007): Merida, Yucatan, Mexico, July 3-11, 2007*, vol. 4, pp. 765–768, 2007.

[60] GAPS collaboration, *Antideuteron Sensitivity for the GAPS Experiment*, *Astropart. Phys.* **74** (2016) 6 [1506.02513].

[61] A. Kounine, *Status of the AMS Experiment*, in *Proceedings, XVI International Symposium on Very High Energy Cosmic Ray Interactions (ISVHECRI 2010), Batavia, IL, USA, 28 June - 2 July 2010*, 2010, 1009.5349.

[62] A. Coogan and S. Profumo, *Origin of the tentative AMS antihelium events*, *Phys. Rev.* **D96** (2017) 083020 [1705.09664].

[63] K. Blum, K. C. Y. Ng, R. Sato and M. Takimoto, *Cosmic rays, antihelium, and an old navy spotlight*, *Phys. Rev.* **D96** (2017) 103021 [1704.05431].

[64] Y.-C. Ding, N. Li, C.-C. Wei, Y.-L. Wu and Y.-F. Zhou, *Prospects of detecting dark matter through cosmic-ray antihelium with the antiproton constraints*, *JCAP* **1906** (2019) 004 [1808.03612].

[65] I. Cholis, T. Linden and D. Hooper, *Anti-Deuterons and Anti-Helium Nuclei from Annihilating Dark Matter*, 2001.08749.

[66] L. A. Dal and M. Kachelrieß, *Antideuterons from dark matter annihilations and hadronization model dependence*, *Phys. Rev.* **D86** (2012) 103536 [1207.4560].

[67] L. A. Dal and A. R. Raklev, *Antideuteron Limits on Decaying Dark Matter with a Tuned Formation Model*, *Phys. Rev.* **D89** (2014) 103504 [1402.6259].

[68] I. Usoskin, "Updated cosmic ray modulation strength (Phi) since 1951 for the LIS by Vos and Potgieter (2015)." Available at http://cosmicrays.oulu.fi/phi/phi.html, 2017.

[69] E. E. Vos and M. S. Potgieter, *New Modeling of Galactic Proton Modulation during the Minimum of Solar Cycle 23/24*, *Astrophys. J.* **815** (2015) 119.

[70] I. G. Usoskin, A. Gil, G. A. Kovaltsov, A. L. Mishev and V. V. Mikhailov, *Heliospheric modulation of cosmic rays during the neutron monitor era: Calibration using PAMELA data for 2006–2010*, *J. Geophys. Res. Space Phys.* **122** (2017) 3875 [1705.07197].